Science Advances
AAAS

Supplementary Materials for

Proteomimetic polymer blocks mitochondrial damage, rescues Huntington's neurons, and slows onset of neuropathology in vivo

Wonmin Choi *et al.*

Corresponding author: Xin Qi, xxq38@case.edu; Nathan C. Gianneschi, nathan.gianneschi@northwestern.edu

Sci. Adv. **10**, eado8307 (2024)
DOI: 10.1126/sciadv.ado8307

This PDF file includes:

Instrumentation
Figs. S1 to S35
Tables S1 to S6

Instrumentation

i. **^{1}H Nuclear Magnetic Resonance (^{1}H NMR)**: ^{1}H NMR spectra were recorded on a Varian Inova spectrometer (500 MHz) in DMF-d_7.

ii. **Analytical High-Performance Liquid Chromatography (HPLC)**: Analytical HPLC analysis of peptides was performed on a Jupiter 4 Proteo 90Å Phenomenex column (150 x 4.60 mm) using a Hitachi-Elite LaChrom L-2130 pump equipped with UV-Vis detector (Hitachi-Elite LaChrom L2420). The solvent system consists of (A) 0.1% TFA in water and (B) 0.1% TFA in acetonitrile.

iii. **Preparative HPLC**: An Armen Glider CPC preparatory HPLC was used to purify all peptides. The solvent system consists of (A) 0.1% TFA in water and (B) 0.1% TFA in acetonitrile.

iv. **Electrospray Ionization Mass Spectrometry (ESI-MS)**: ESI-MS spectra of peptides were collected using a Bruker Amazon-SL spectrometer configured with an ESI source in both negative and positive ionization mode.

v. **Matrix Assisted Laser Desorption Ionization – Time of Flight Mass Spectrometry (MALDI-ToF MS)**: MALDI-ToF MS spectra of polymers in CHCA matrix were collected using a Bruker AutoFlex III Smartbeam spectrometer in both negative and positive ionization modes.

vi. **Organic Phase Gel Permeation Chromatography (Organic GPC)**: Organic phase GPC measurements were performed on a set of Phenomenex Phenogel 5m, 1K-75K, 300 x 7.80 mm in series with a Phenomex Phenogel 5m, 10K-1000K, 300 x 7.80 mm columns with HPLC grade solvents as eluents: dimethylformamide (DMF) with 0.05 M of LiBr at 60 °C. Detection consisted of a Hitachi UV-Vis Detector L-2420, a Wyatt Optilab T-rEX refractive index detector operating at 658 nm and a Wyatt DAWN® HELEOS® II light scattering detector operating at 659 nm. Absolute molecular weights and polydispersities were calculated using the Wyatt ASTRA software with dn/dc values determined by assuming 100% mass recovery during GPC analysis.

vii. **Aqueous Phase Gel Permeation Chromatography (Aqueous GPC)**: Aqueous phase GPC measurements were performed on an Agilent 1200 HPLC system with a PSS Suprema column using HPLC grade water with 0.1% trifluoroacetic acid buffer as the mobile phase. Detection consisted of a Wyatt Optilab T-rEX refractive index detector operating at 658 nm and a Wyatt DAWN® HELEOS® II light scattering detector operating at 659 nm. Absolute molecular weights and polydispersities were calculated using the Wyatt ASTRA software with dn/dc values determined by assuming 100% mass recovery during GPC analysis.

viii. **Flow Cytometry:** Cellular uptake of P1/HV3-TAT was analyzed via flow cytometry using a BD FacsAria IIu 4-Laser flow cytometer (Becton Dickinson Inc., USA). Mean fluorescence intensity were prepared for presentation using FlowJo v10.

ix. **Confocal Laser Scanning Microscopy (CLSM)**: Imaging was accomplished using LEICA SP5 II laser scanning confocal microscope with a 40x oil immersion objective. The cell nuclei (stained with Hoechst) was accomplished using a 358 nm laser with a 15% laser power. Cell imaging for the membrane (stained with wheat germ agglutinin) was accomplished using a 488 nm laser with an 12% laser power. Rhodamine-labeled P1 and HV3-TAT were imaged using a 561nm laser with 12% laser power.

x. **Fluorescence Measurement**: CellTiter-Blue® fluorescence measurements were recorded using a Perkin Elmer EnSpire multimode Plate Reader.

xi. **Cell Culture:** HdhQ111 cells originally purchased from the Coriell Institute. Cells were incubated at 33˚C at 5% CO2 using DMEM (high glucose, no glutamine, Life Technologies/Gibco, Cat. 11960044) supplemented with 10% FBS (heat inactivated, Omega Scientific, Cat FB-02), and 1x of sodium pyruvate (100x = 100mM, Life Technologies, Cat. 11360070), G-418 Disulfate (DOT Scientific, DSG64500), GlutaMAX (Life technologies, Cat. 35050061) and antibiotics (Penicillin-Streptomycin, Life Technologies Cat 15140122). Cell cultures were maintained by subculturing in flasks every 4-7 days when cells became confluent using trypsin-EDTA, 0.25% (Life Technologies, Cat 25200114).

xii. **Animal Care:** Mice (CD1, C57BL/6J, R6/2) for in vivo studies were obtained from the Jackson Laboratory. All animal procedures were approved by NU's institutional animal care and use committee (IACUC) and performed by Developmental Therapeutics Core if done at Northwestern. For Case Western studies, all animal studies were conducted in accordance with protocols approved by the Institutional Animal Care and Use Committee of Case Western Reserve University and were performed based on the NIH Guide for the Care and Use of Laboratory Animals. Sufficient procedures were employed for reducing pain or discomfort of mice during the experiments.

xiii. **ICP-MS:** Inductively couple plasma mass spectrometry (ICP-MS) was performed at the Northwestern University Quantitative Bioelemental Imaging Core on the Thermo iCAP Q ICP-MS, controlled using QTEGRA software.

List of Figures

Figure S1. Characterization of HV3 peptide monomer library
Figure S2. Polymerization kinetics of HV3 peptide monomers
Figure S3. Percent conversion and log plots of polymerization of HV3 monomers
Figure S4. SEC-MALS characterization of HV3-PLPs
Figure S5. SEC-MALS trace for P1 Batch used for behavioral and toxicity studies and SDS PAGE gel for P1 batch used in *in vivo* efficacy studies
Figure S6. Western blot for VCP protein association
Figure S7. Characterization of rhodamine labeled HV3-TAT peptide (HV3-TAT-Rho)
Figure S8. Characterization of rhodamine labeled P1 PLP (P1-Rho)
Figure S9. Live cell confocal microscopy in HdhQ111 cells showing cell penetration.
Figure S10. Cell penetration assessed by split channels of live-cell confocal microscopy images of HdhQ111 cells treated with (A) HV3-TAT-Rho and (B) P1-Rho
Figure S11. Live-cell confocal microscopy of HdhQ111 cells treated with rhodamine dye alone (3uM) to assess cell penetration
Figure S12. Raw flow cytometry data showing cellular uptake in HdhQ111 cells following treatment with HV3-TAT-Rho peptide, P1-Rho, rhodamine dye, and vehicle
Figure S13. Accumulation assay in mouse striatal HdhQ111 cells
Figure S14. Mitochondrial localization assessed by split channels of live-cell confocal microscopy images of HdhQ111 cells treated with (A) HV3-TAT-Rho and (B) P1-Rho
Figure S15. Live-cell confocal microscopy of HdhQ111 cells treated with rhodamine dye alone (3 µM) to assess mitochondrial localization
Figure S16. *In vitro* binding affinity of HV3-TAT and P1 to VCP protein using Biolayer interferometry (Blitz) measurements
Figure S17. SDS-PAGE assay for assessing enzyme degradation resistance of P1
Figure S18. Enzymatic degradation assay using HPLC
Figure S19. Percentage cleavage of P1 and HV3-TAT over time after enzyme and serum treatment, analyzed by HPLC.
Figure S20. Serum degradation assay using HPLC
Figure S21. Characterization EDANS-DABCYL conjugated monomer
Figure S22. Polymerization of EDANS-DABCYL conjugated monomer (M1-ED)
Figure S23. Enzyme degradation kinetics of fluorogenic monomer (M1-ED) and PLP (P1-ED)
Figure S24. Liver microsome degradation assay
Figure S25. Cell viability assay with enzyme and serum pretreated HV-3 TAT peptide and P1
Figure S26. Synthetic scheme of DOTA-TA
Figure S27. Characterization of DOTA-TA
Figure S28. Termination of polymerization with DOTA-TA
Figure S29. Synthetic scheme of Gd-DOTA-TA
Figure S30. Gd-DOTA-TA Characterization
Figure S31. Linear calibration of Gd to PLP and SEC-MALS trace of Gd-PLP
Figure S32. Time-course concentration of Gd-P1 in different brain regions
Figure S33. Complete Blood Count for Toxicity Analysis, corresponding to Supplementary Table S3

Figure S34. Biochemistry Blood Profile for Toxicity Analysis, corresponding to Supplementary Table S4
Figure S35. Full blot image of the IB: BDNF line from Fig. 6a.
Table S1. Polymer characterization for figures
Table S2. Statistical analysis of Gd-P1 pharmacokinetic output and detailed Cle, Clp, Vc, and Vp
Table S3. Complete blood count panel
Table S4. Blood chemistry panel
Table S5. Abbreviations for CBC and blood chemical analyses
Table S6. Severity scoring of toxicity pathology

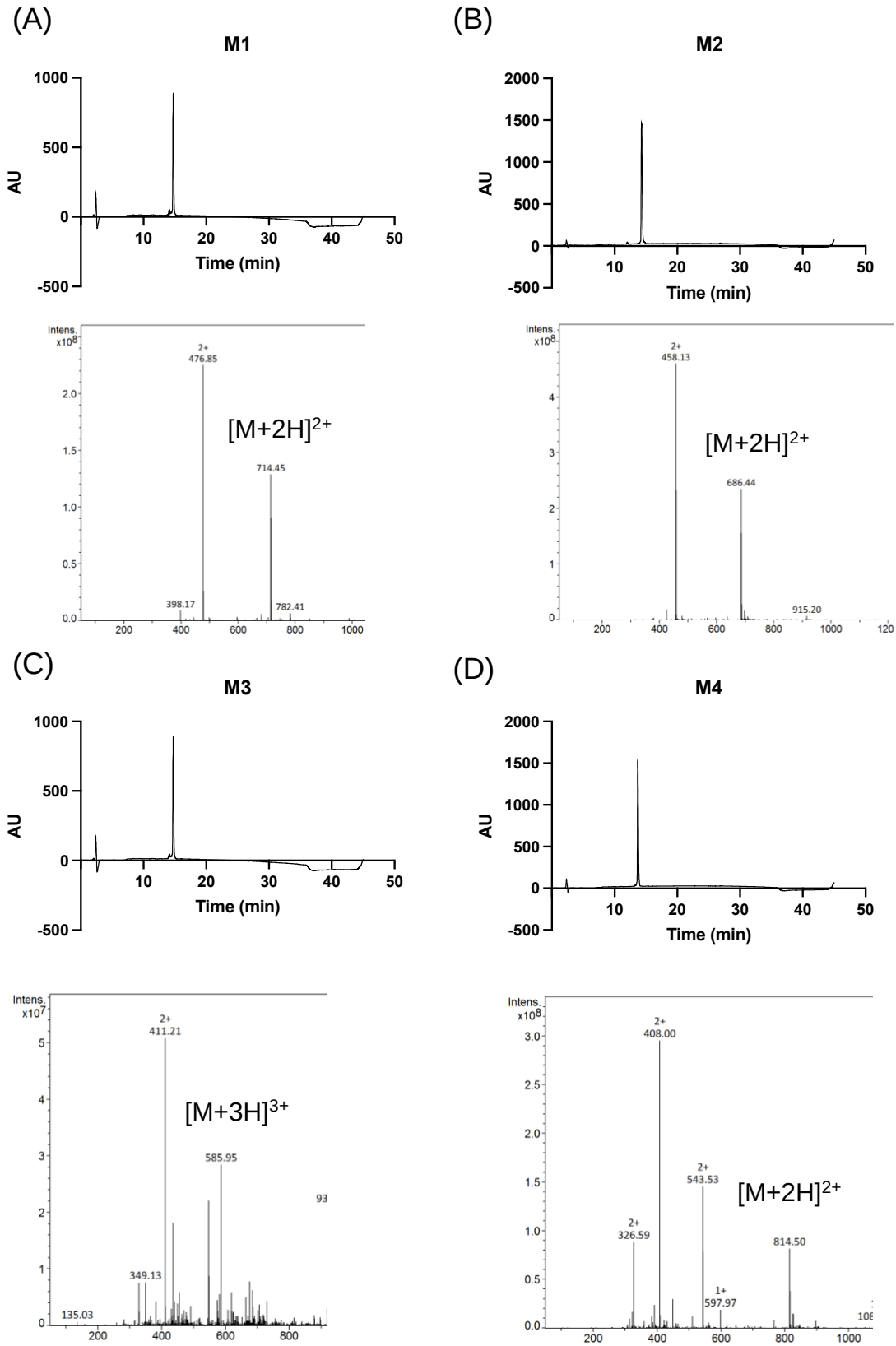

Figure S1. Characterization of HV3 peptide monomer library. Analytical HPLC trace (above) and ESI-MS (below) of (A) M1, (B) M2 (C) M3 and (D) M4.

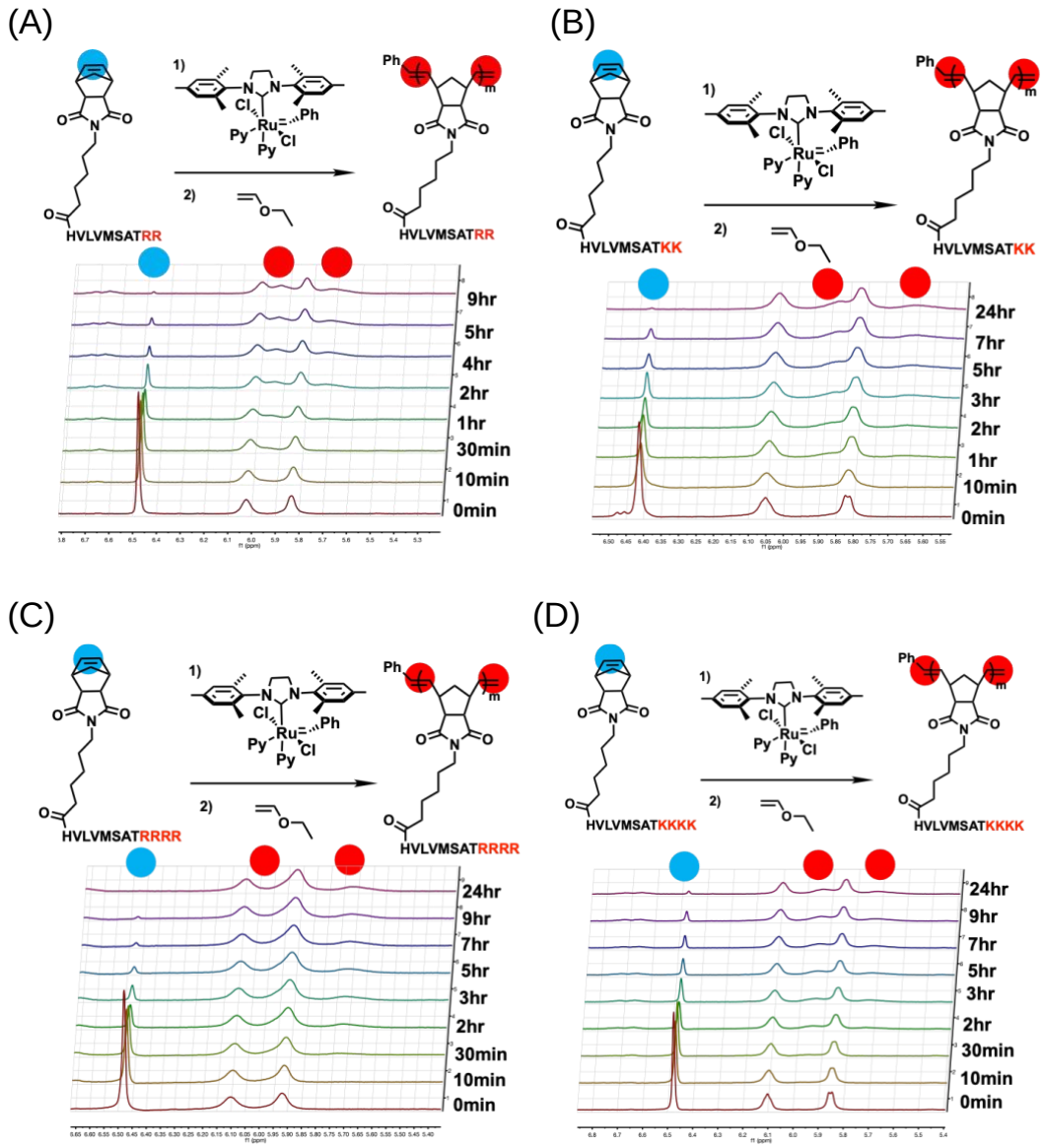

Figure S2. Polymerization kinetics of HV3 peptide monomers. Polymerization kinetics of HV3 peptide monomers with different positive charged amino acids were monitored by NMR. The absence of the olefin proton peak (blue circle) from the **δ** = 6.45 ppm and the corresponding appearance of two broad cis- and trans- olefin proton peaks (red circle) from **δ** = 5.8 – 6.0 ppm presents the completion of the polymerization reaction. (A) HV3 monomer with two arginines (M1), (B) HV3 monomer with two lysines (M2), (C) HV3 monomer with four arginines (M3), (D) HV3 monomer with four lysines (M4).

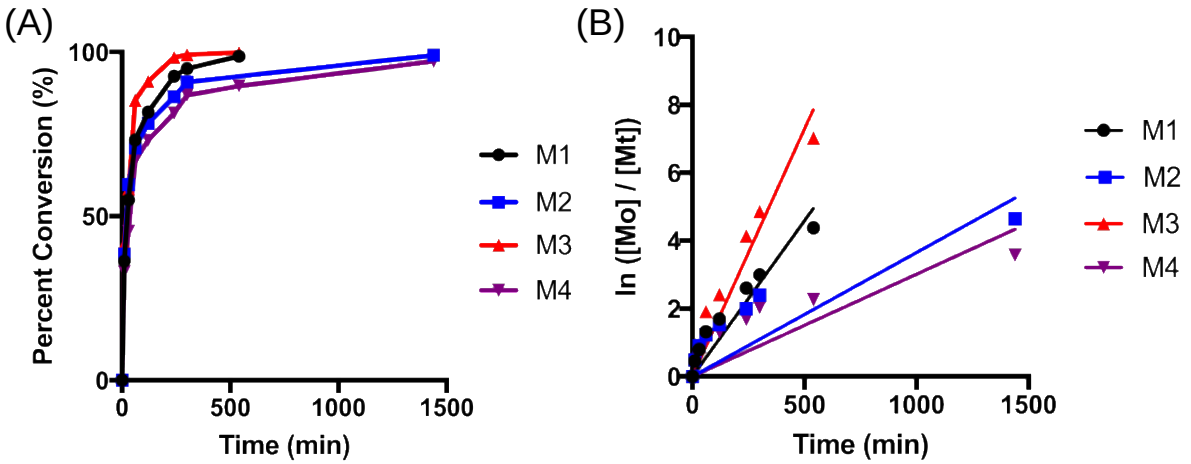

Figure S3. Percent conversion and log plots of polymerization of HV3 monomers. (A) Percent conversion of monomers determined by integration of olefin peaks in ^{1}H NMR (B) Log plots of the polymerization of each monomer. The following slopes (k_{obs}) were determined by linear lease-squares fitting of the plots : 0.0329 min^{-1} (M1) 0.0154 min^{-1} (M2) 0.0119 min^{-1} (M3) 0.0076 min^{-1} (M4).

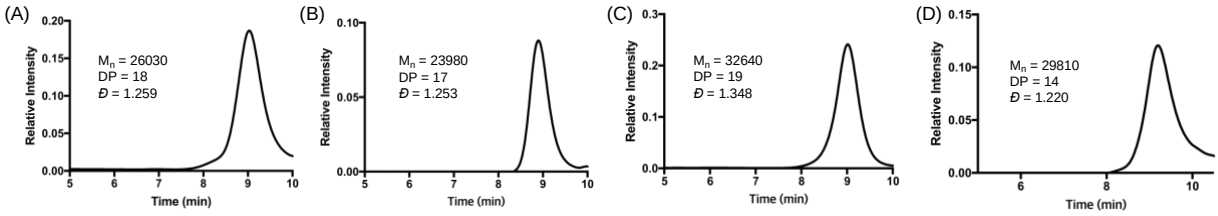

Figure S4. SEC-MALS characterization of HV3-PLPs. SEC-MALS trace determining molecular weight, DP and dispersity (*Đ*) of (A) P1 (B) P2 (C) P3 and (D) P4.

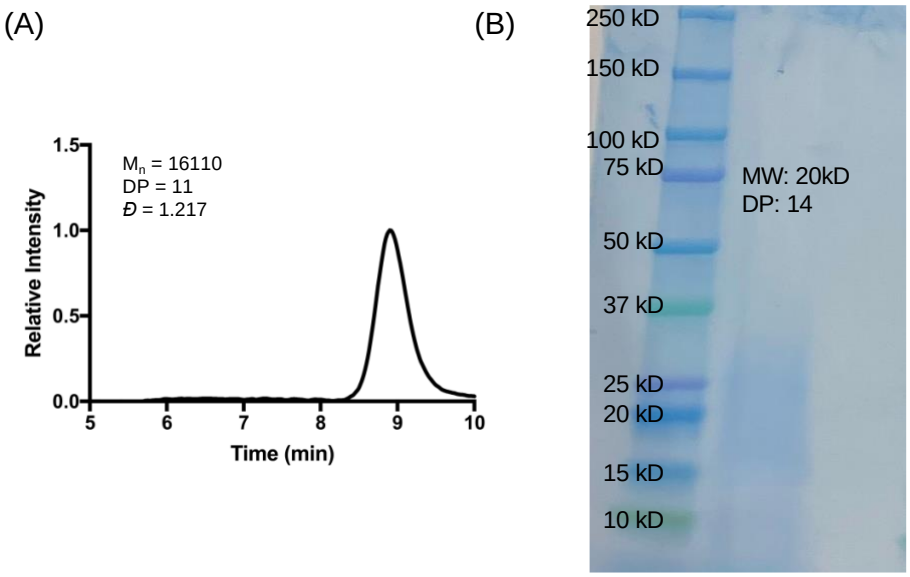

Figure S5. SEC-MALS trace for P1 Batch used for behavioral and toxicity studies and SDS PAGE gel for P1 batch used in in vivo efficacy studies.

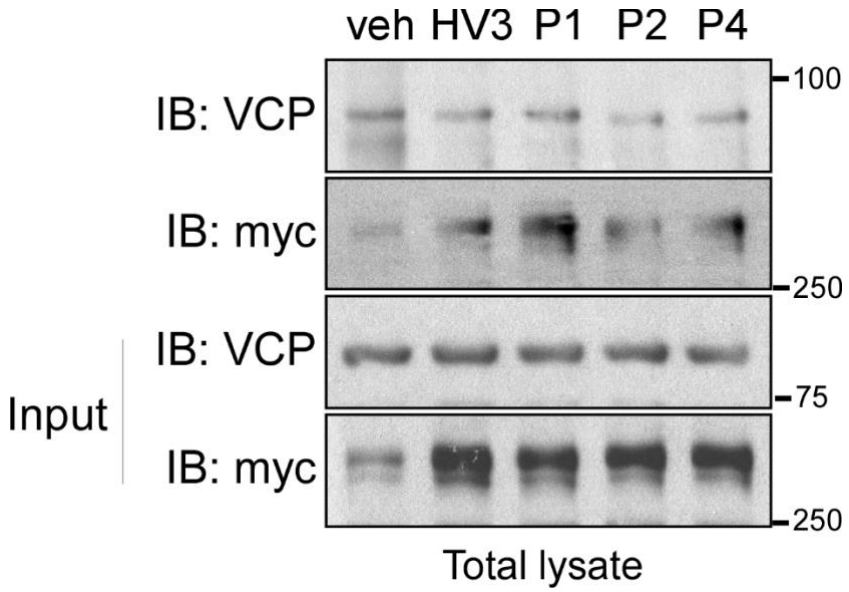

Figure S6. Representative Western Blot image from of VCP/myc association assay showcasing the vehicle, HV3-TAT, P1, P2, and P4 results.

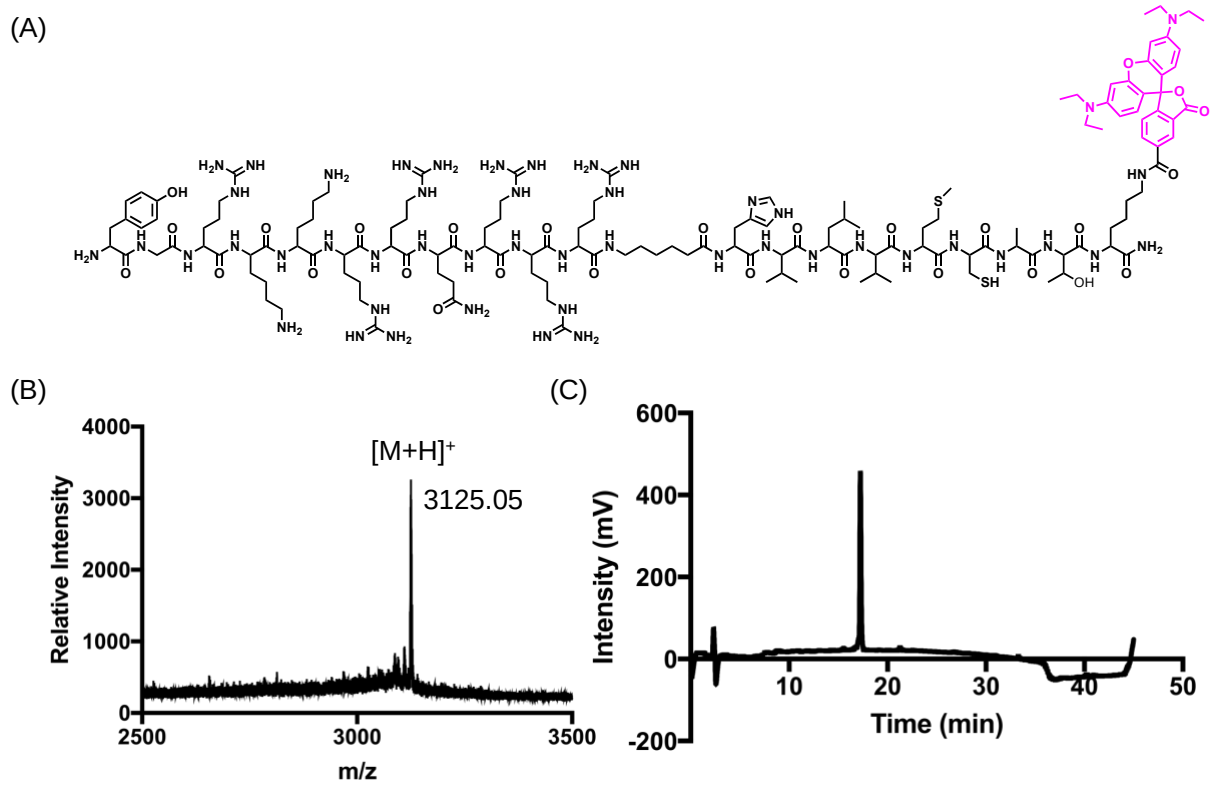

Figure S7. Characterization of rhodamine labeled HV3-TAT peptide (HV3-TAT-Rho). (A) Chemical structure of rhodamine labeled HV3-TAT peptide. (B) MALDI-TOF trace determining molecular weight of rhodamine labeled HV3-TAT peptide. (C) HPLC trace of rhodamine labeled HV3-TAT peptide.

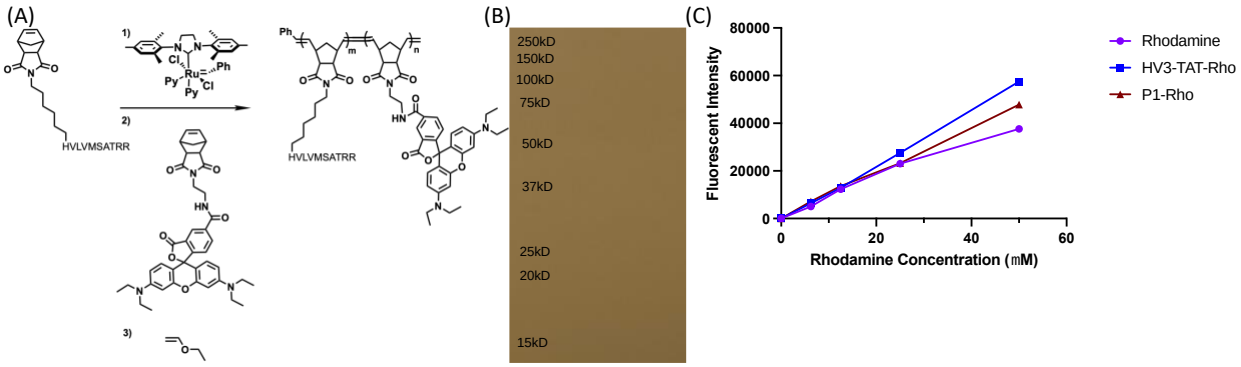

Figure S8. Characterization of rhodamine labeled P1 PLP (P1-Rho). (A) Chemical structure of rhodamine labeled P1 PLP. (B) SDS PAGE determining molecular weight of rhodamine labeled P1 PLP. (C) Fluorescent spectroscopy of HV3-TAT-Rho, P1-Rho, and Rhodamine showing near 1:1 addition of dye on to compounds.

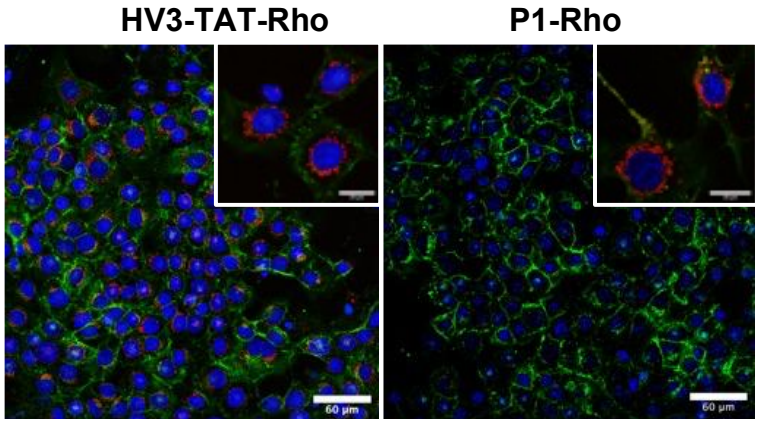

Figure S9. Live cell confocal microscopy in HdhQ111 cells showing cell penetration. HdhQ111 cells were treated with HV3-TAT peptide or **P1** at a concentration of 3 µM with respect to peptide. Cell Membrane: wheat germ agglutinin-Alexa 488 (green channel). Material: Rhodamine (red channel). Nuclei: Hoechst 33342 stain (blue channel). Scale Bars: 60 µm; 20 µm for inset.

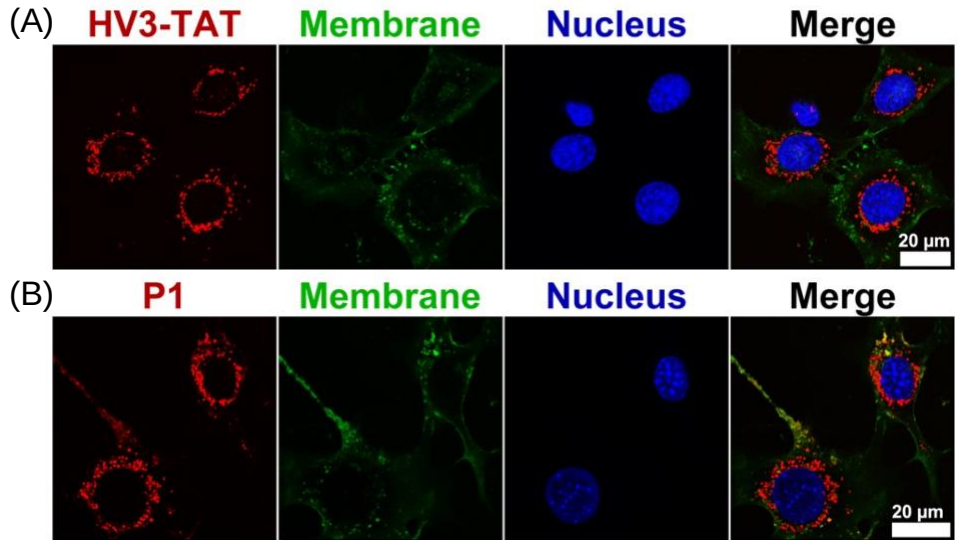

Figure S10. Cell penetration assessed by split channels of live-cell confocal microscopy images of HdhQ111 cells treated with (A) HV3-TAT-Rho and (B) P1-Rho. Material: Rhodamine (red channel). Cell Membrane: wheat germ agglutinin-Alexa 488 (green channel). Nuclei: Hoechst 33342 stain (blue channel). Scale: 20 µm.

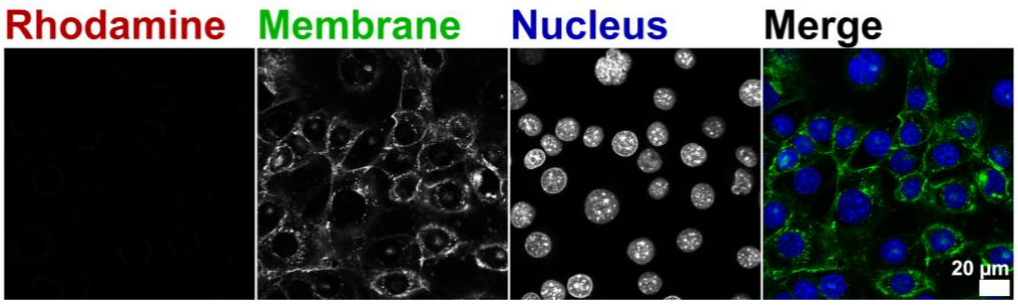

Figure S11. Live-cell confocal microscopy of HdhQ111 cells treated with rhodamine dye alone (3uM) to assess cell penetration. Rhodamine dye: red channel. Cell membrane: wheat germ agglutinin-Alexa 488 (green channel). Nuclei: Hoechst 33342 stain (blue channel).

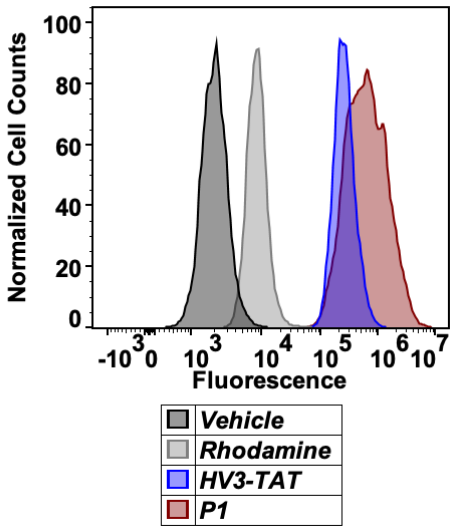

Figure S12. Raw flow cytometry data showing cellular uptake in HdhQ111 cells following treatment with HV3-TAT-Rho peptide, P1-Rho, rhodamine dye, and vehicle.

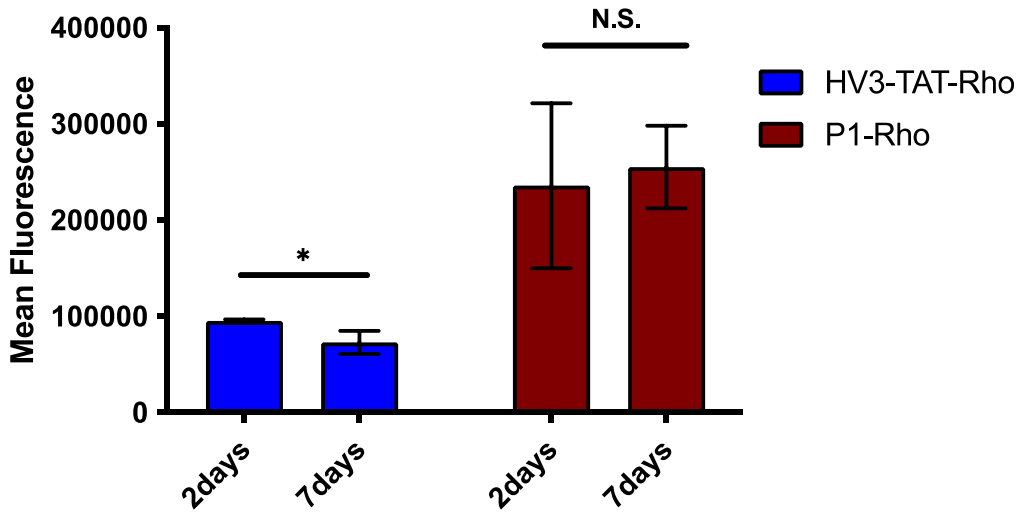

Figure S13. Accumulation assay in mouse striatal HdhQ111 cells. (A) Quantification of mean fluorescence output of flow cytometry in mouse striatal HdhQ111 cells reporting presence of compounds 2 and 7 days post single treatment. Unpaired t-test between groups was performed. Statistical significance was defined as follows : *N.S.* ($p > 0.05$), * ($p \leq 0.05$), ** ($p \leq 0.01$), *** ($p \leq 0.001$), and **** ($p \leq 0.0001$).

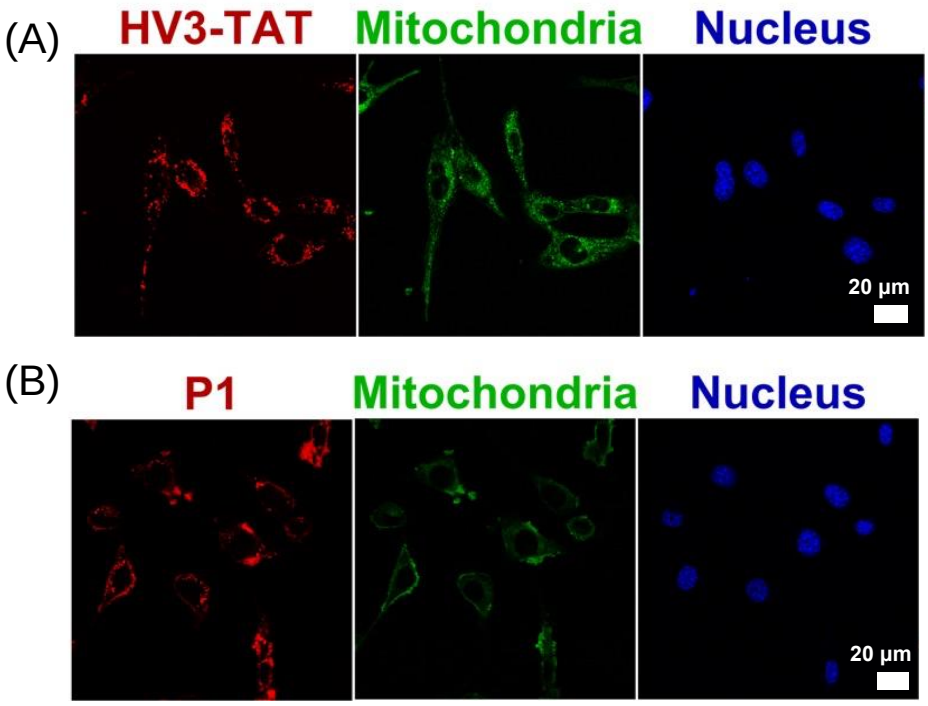

Figure S14. Mitochondrial localization assessed by split channels of live-cell confocal microscopy images of HdhQ111 cells treated with (A) HV3-TAT-Rho and (B) P1-Rho. Material: Rhodamine (red channel). Mitochondria: Mitotracker Green FM (green channel). Nuclei: Hoechst 33342 stain (blue channel). The merged images can be found in **Fig. 2d**. Scale: 20 µm.

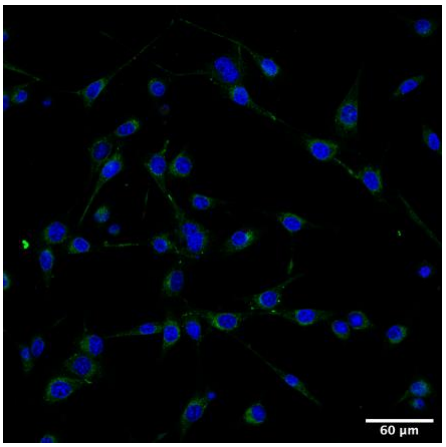

Figure S15. Live-cell confocal microscopy of HdhQ111 cells treated with rhodamine dye alone (3 µM) to assess mitochondrial localization. Mitochondria: Mitotracker Green FM (green channel). Nuclei: Hoechst 33342 stain (blue channel). Rhodamine dye: red channel.

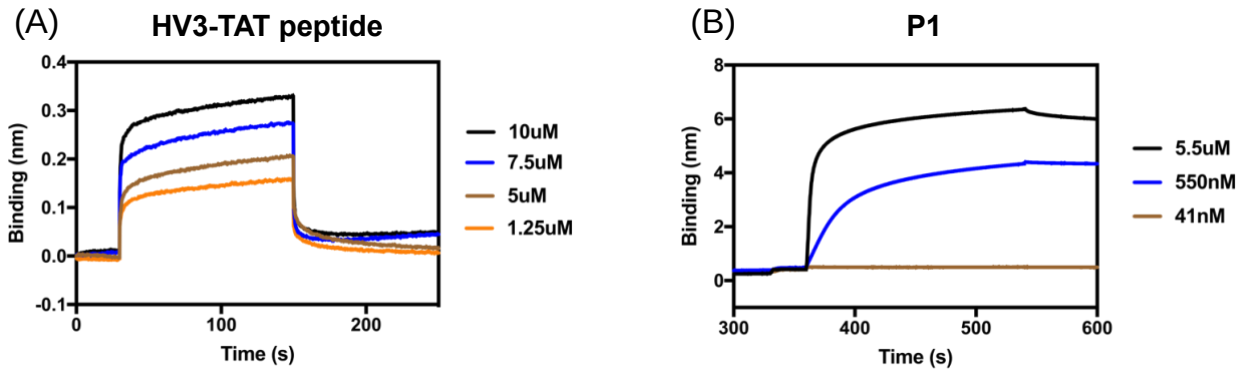

***Figure S16. In vitro* binding affinity of HV3-TAT and P1 to VCP protein using Biolayer Interferometry (BLItz) measurements.** The representative binding responses over time of (A) HV3-TAT and (B) P1 using biosensors loaded with VCP proteins, incubated different concentrations.

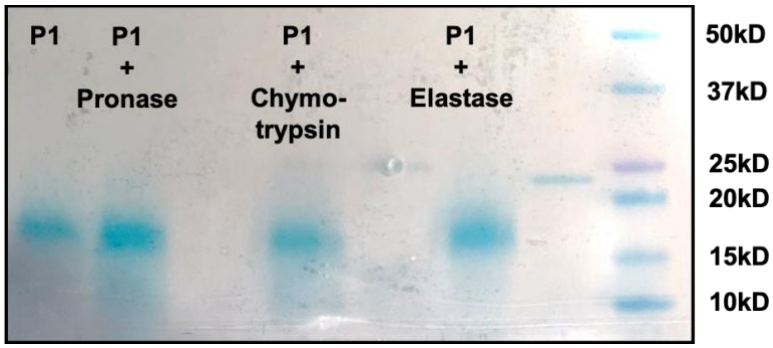

Figure S17. SDS-PAGE assay for assessing enzyme degradation resistance of P1. P1 was pretreated with three different enzymes (pronase, chymotrypsin, elastase) for 1 hr prior to analysis.

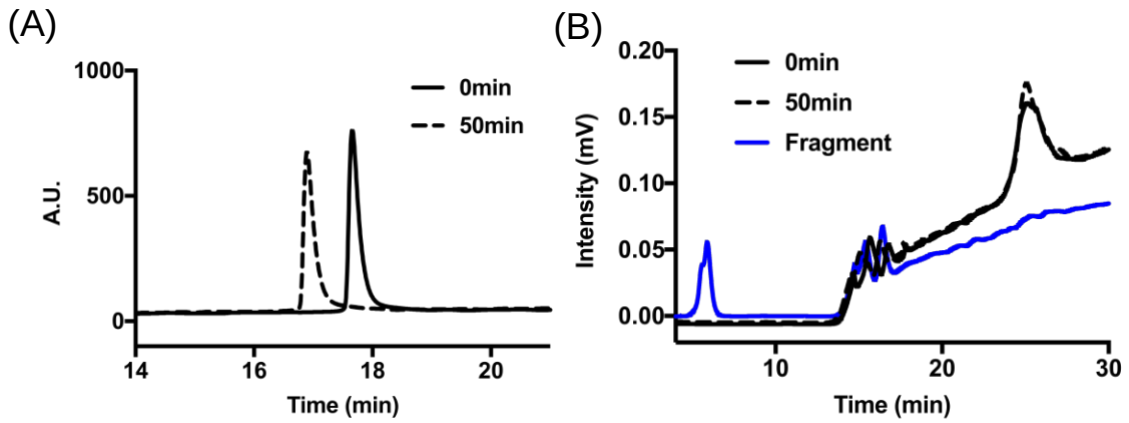

Figure S18. Enzyme degradation assay using HPLC. The degradation kinetics of both HV3-TAT and P1 under the treatment of pepsin (pH2) was monitored by HPLC (A,B). (A) HV3-TAT (solid line) was degraded into cleaved product (dashed line). (B) P1 (solid line) was not degraded after the incubation in the pepsin enzyme for 50 minutes (dashed line). Expected fragment peak didn't overlap with dashed line (blue line, sequence = SATRR), indicating that there is no degradation of P1.

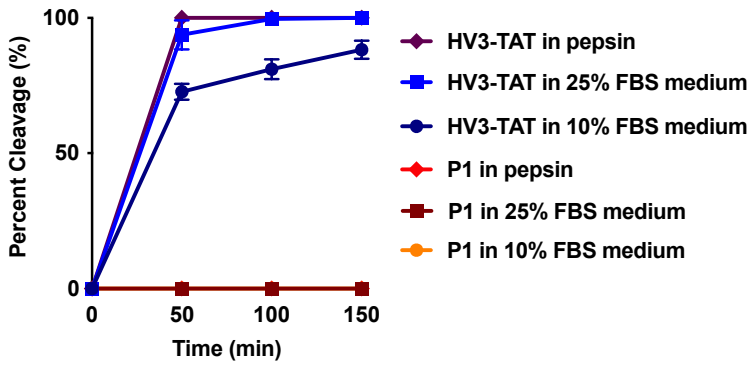

Figure S19. Percentage cleavage of P1 and HV3-TAT over time after enzyme and serum treatment, analyzed by HPLC. **P1** and HV3-TAT peptide were pretreated with pepsin, 25% fetal bovine serum rich medium, and 10% fetal bovine serum rich medium for 150 min with aliquots tested at time points shown (n=3).

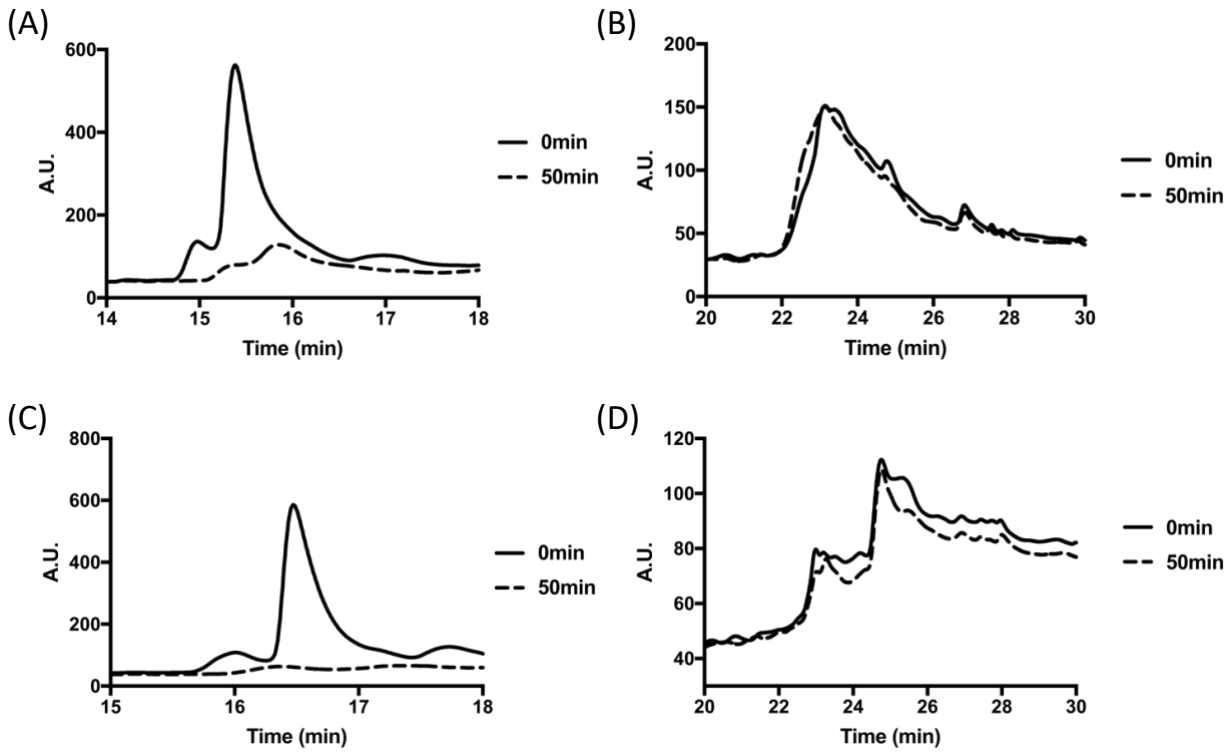

Figure S20. Serum degradation assay using HPLC. The degradation kinetics of both HV3-TAT and P1 under the treatment of 10% FBS (A,B) or 25% FBS (C,D) was monitored by HPLC. HV3-TAT (solid line in panels A and C) exhibited degradation within 50 minutes (dashed line in panels A and C) when incubated with 10% FBS (A) and 25% FBS (C). In contrast, P1 (solid line in panels B and D) remained undegraded even after 50 minutes of incubation with 10% FBS (B) and 25% FBS (D) (dashed line in panels B and D).

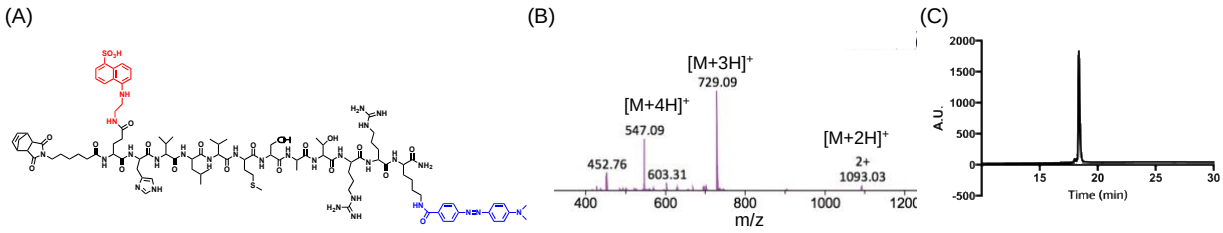

Figure S21. Characterization EDANS-DABCYL conjugated monomer. (A) Chemical structure of EDANS-DABCYL conjugated HV3 Peptide monomer 1 (M1-ED). EDANS (red)-glutamic acid and DABCYL(blue)-lysine was added to the original monomer 1 (M1) sequence. (B) Mass of M1-ED was confirmed by ESI-MS. (C) RP-HPLC trace of M1-ED.

3.15 Synthesis of P1- EDANS-DABCYL polymer

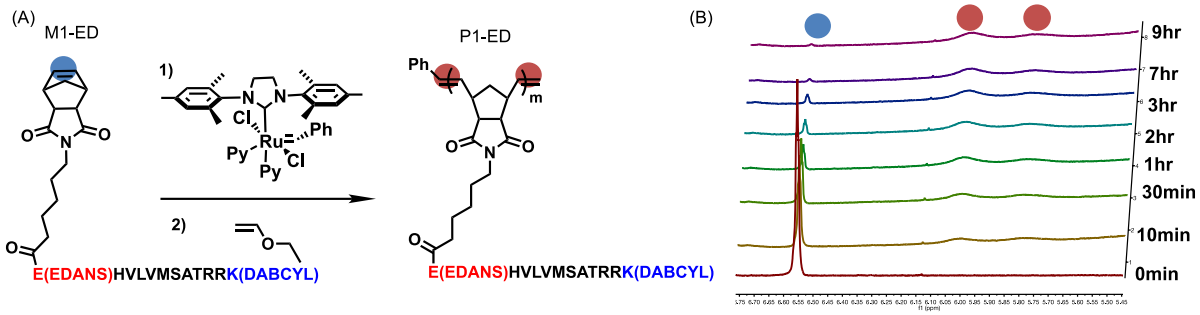

Figure S22. Polymerization of EDANS-DABCYL conjugated monomer (M1-ED). (A) Polymerization scheme of M1-ED. M1-ED monomer was polymerized into EDANS-DABCY conjugated HV3-PLP (P1-ED). (B) Polymerization kinetics of M1-ED. The absence of the olefin proton peak (blue circle) from the **δ** = 6.55 ppm and the corresponding appearance of two broad cis- and trans- olefin proton peaks (orange circle) from **δ** = 5.8 – 6.0 ppm presents the completion of the polymerization reaction.

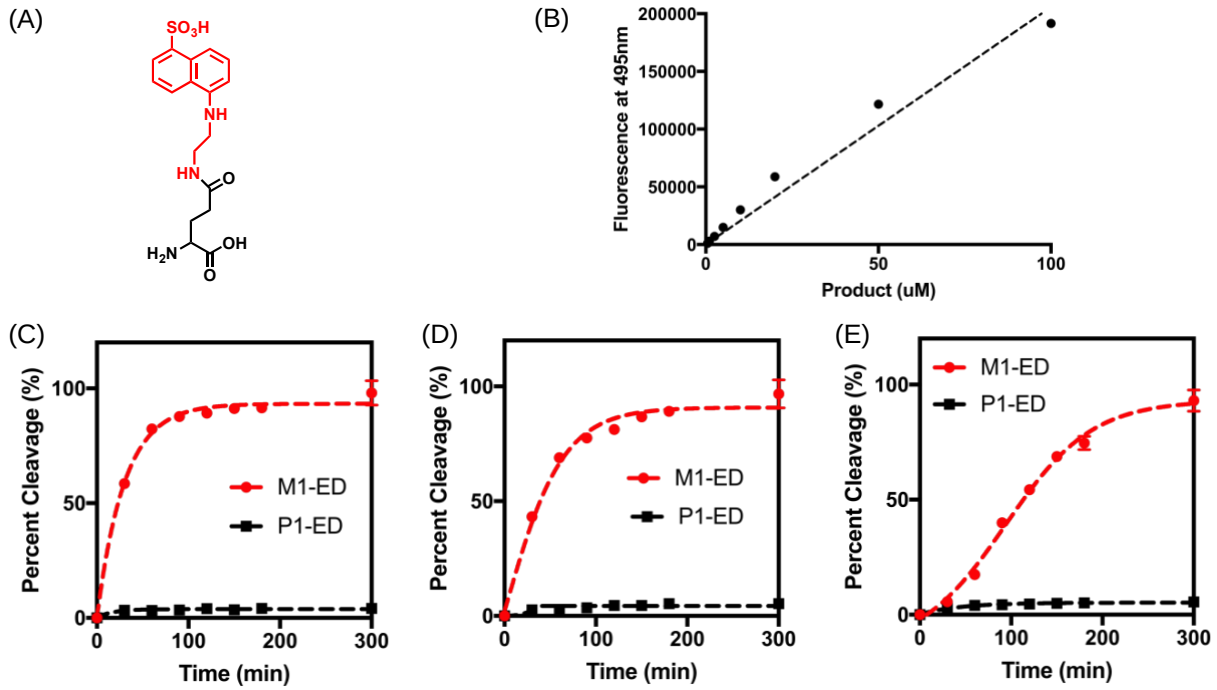

Figure S23. Enzyme degradation kinetics of fluorogenic monomer (M1-ED) and PLP (P1-ED). (A) Chemical structure of EDANS-glutamic acid. (B) Calibration curve of EDANS-glutamic acid. EDANS-glutamic acid with different concentration was excited at 340nm and emitted at 495nm on a plate reader. Time course enzyme degradation of fluorogenic HV3 monomer (M1-ED) and HV3-PLP (P1-ED) by (C) trypsin, (D) thermolysin, and (E) elastase, respectively. The fluorescence was measured at 495nm by plate reader and the percent cleavage was calculated based on the calibration curve (B).

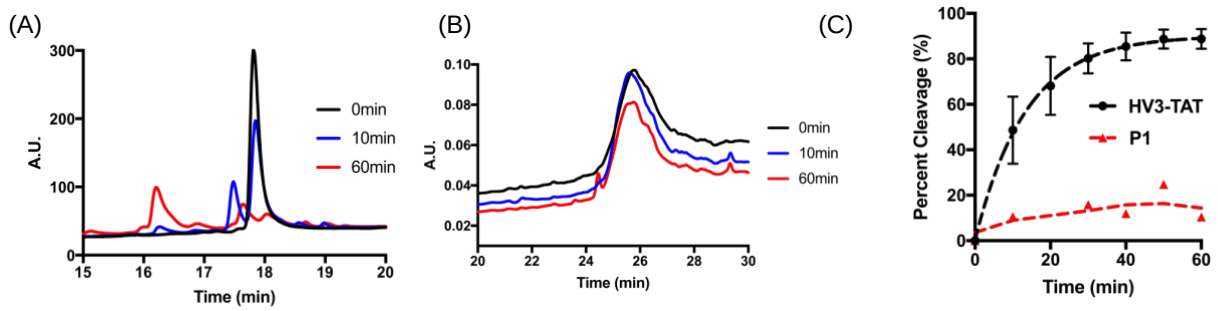

Figure S24. Liver microsome degradation assay. (A) RP-HPLC trace of HV3-TAT after the incubation in the liver microsome. (B) RP-HPLC trace of P1 after the incubation in the liver microsome. (C) Percent cleavage kinetics of HV3-TAT and P1 in the liver microsome.

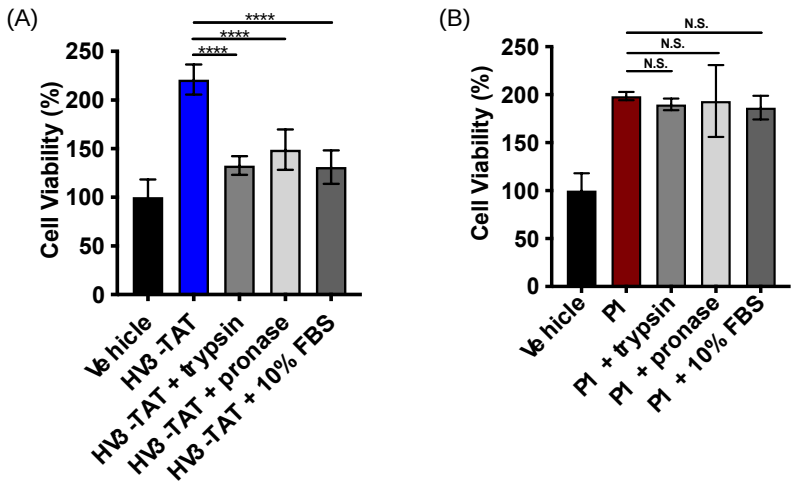

Figure S25. Cell viability assay with enzyme and serum pretreated HV-3 TAT peptide and P1. (A) HV3-TAT peptide and (B) **P1** were pretreated with trypsin, pronase, and 10% fetal bovine serum rich medium for 1 hr before using them to treat HdhQ111cells. Cell viability was analyzed 72 hr post treatment. *One-way ANOVA comparisons of the mean of each group to HV3-TAT (A) and P1 (B) was used for analysis. Statistical significance was defined as follows: N.S. ($p > 0.05$), * ($p \leq 0.05$), ** ($p \leq 0.01$), *** ($p \leq 0.001$), and **** ($p \leq 0.0001$). Values are mean ± SEM.*

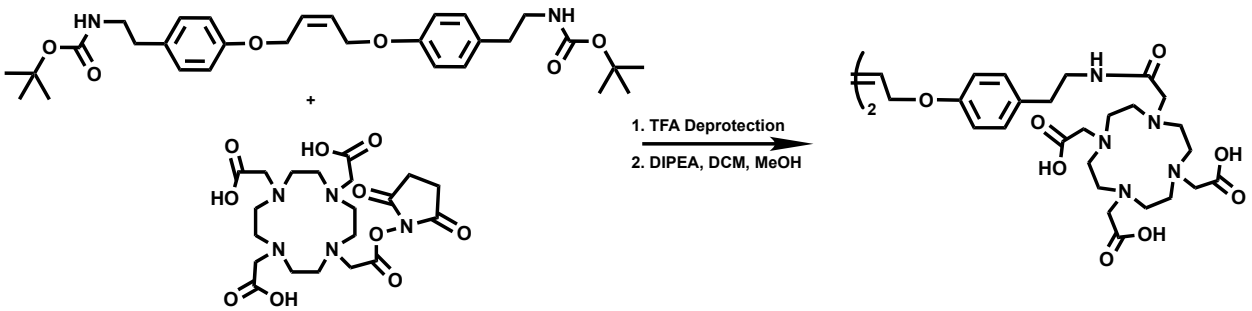

Figure S26. Synthetic scheme of DOTA-TA. 51.69 mg (0.10375 mmol) 4,4'-[(2Z)-2-Butene-1,4-diylbis(oxy)]bis[benzeneethanamine] (prepared via methods from previous report[2]) was deprotected with 3 ml of TFA in 3 mL of DCM for 2 h and rotovapped to leave a brown oil, and then mixed with DOTA-NHS Ester (Macrocyclics, B-280), 158 mg (0.2075 mmol) in DIPEA (5 mL) and DCM (5 mL) and MeOH (1 mL). The reaction mixture was stirred at room temperature for 48 h. Solvent was removed *in vacuo* leaving a brown oil.

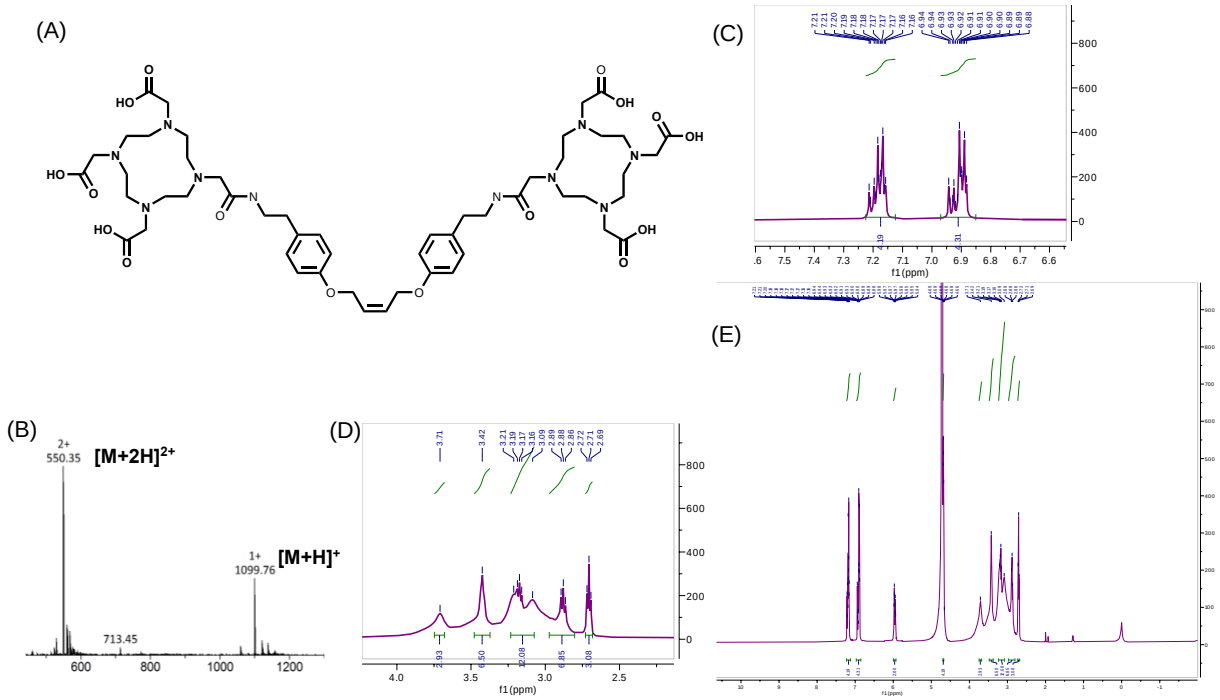

Figure S27. Characterization of DOTA-TA. (A) Chemical structure of DOTA-TA (B) Mass of DOTA-TA confirmed by ESI-MS. (C-E) NMR spectra of DOTA-TA. NMR peaks: 1H NMR-D_2O- 7.25-6.85(m, 8H), 5.9 (m, 2H), 4.7 (m,4H), 4.1-2.6(m, 32H), 2 (s, 1H), 1.9 (s, 1H)

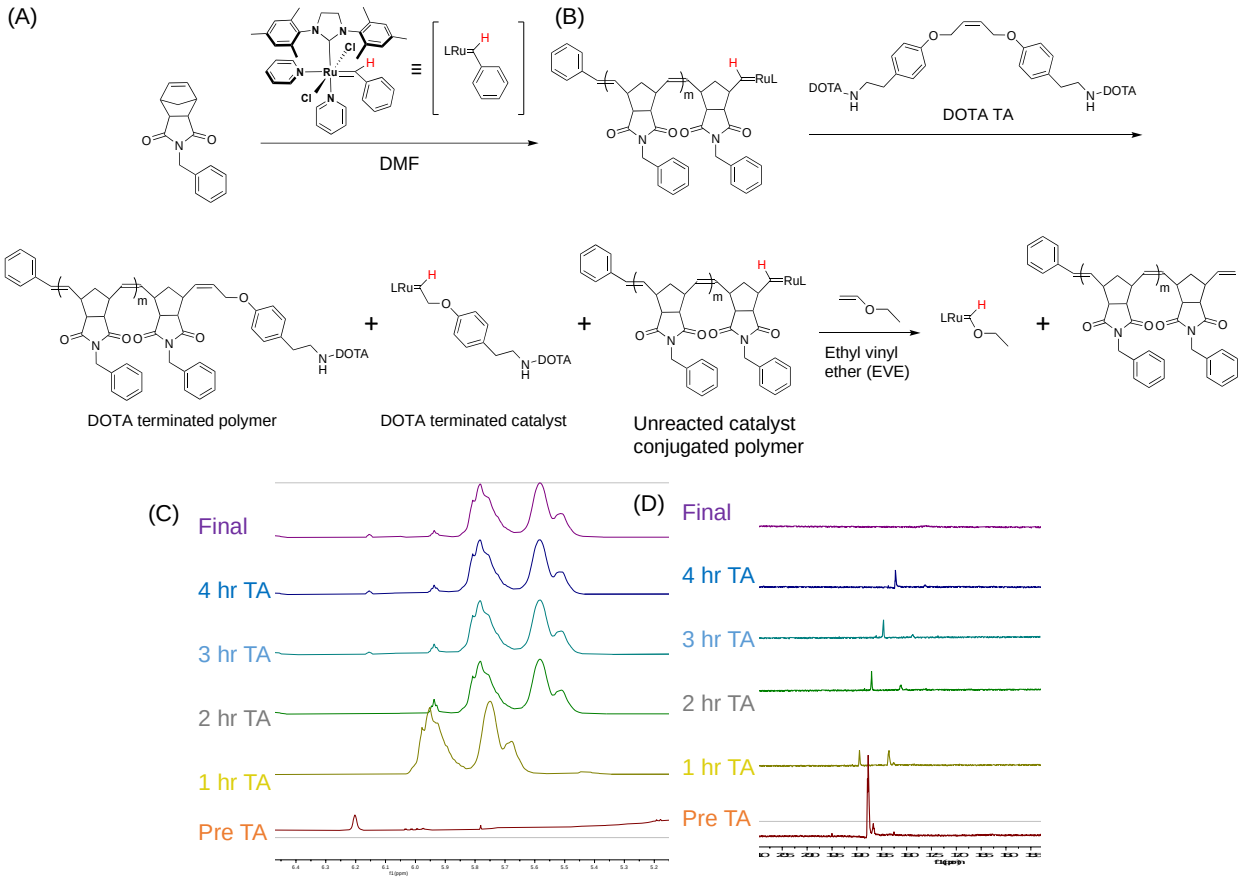

Figure S28. Termination of polymerization with DOTA-TA. (A) Polymerization and termination scheme of phenyl-norbornene. Polymerization was terminated by DOTA-TA yielding DOTA terminated polymer. DOTA terminated catalyst and unreacted catalyst conjugated polymer were quenched by ethyl vinyl ether. (B) Polymerization kinetics of phenyl norbornene. The absence of the monomer olefin proton peak (green circle) from the **δ** = 6.55 ppm and the corresponding appearance of two broad cis- and trans- olefin proton peaks (blue circles) from **δ** = 5.8 – 6.0 ppm presents the completion of the polymerization reaction. (C). The reduction of the catalyst-monomer olefin proton peak (red circle) from the **δ** = 18.75 ppm to **δ** = 17.75 ppm and the corresponding appearance of catalyst-terminating agent olefin proton peak (purple circle) at **δ** =19 ppm presents the termination of the polymerization reaction.

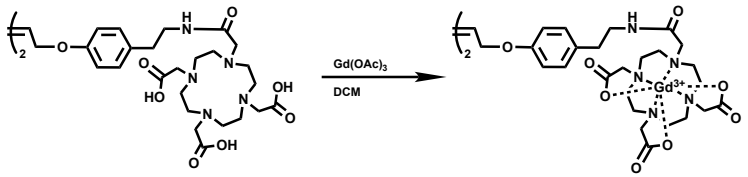

Figure S29. Synthetic scheme of Gd-DOTA-TA. DOTA-TA (35.92 mg) was dissolved in DCM (5 mL), and 2 eq. $Gd(OAc)_3$ added (25.87 mg, 0.0656 mmol). Reaction stirred for 48 hr at room temperature. Solvent was removed in vacuo to yield Gd-DOTA-TA as a white microcrystalline solid. This powder was purified using preparative HPLC on a gradient of 25%-35% Buffer B (MeCN with 0.1% TFA) in Buffer A (Water with 0.1% TFA). Purified, lyophilized product was characterized via ESI and RP-HPLC. Gd metalation efficiency was confirmed via ICPM-MS. Briefly, 0.68 mg of Gd-DOTA-TA was weighed and digested overnighted, diluted and then run on ICP-MS where metalation efficiency was determined to be 98.99%.

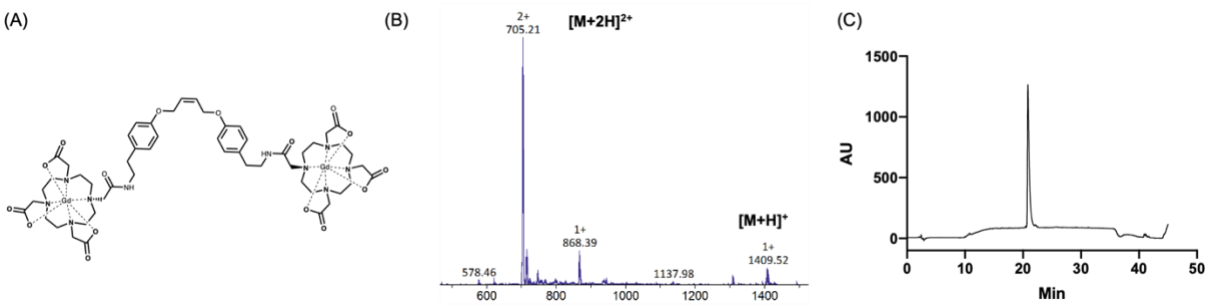

Figure S30. Gd-DOTA-TA characterization. (A) Chemical structure of Gd-DOTA-TA (B) Mass of Gd-DOTA-TA confirmed by ESI-MS. (C) RP-HPLC trace of Gd-DOTA-TA.

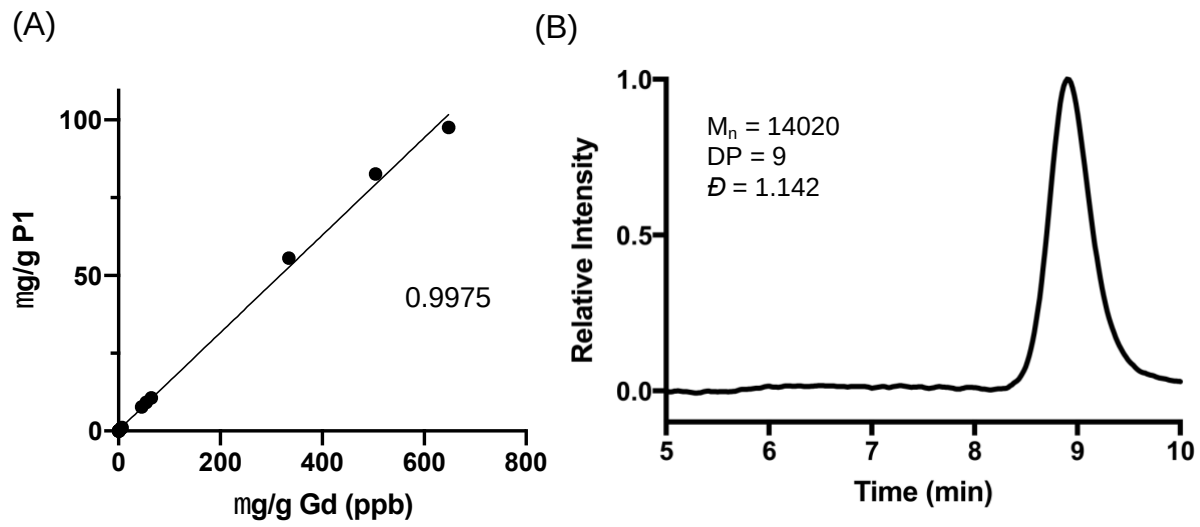

Figure S31. Linear calibration of Gd to PLP and SEC-MALS trace of Gd-PLP. (A) Calibration curve of Gd-P1 ICPMS after blood digestion (B) SEC-MALS of Gd-P1.

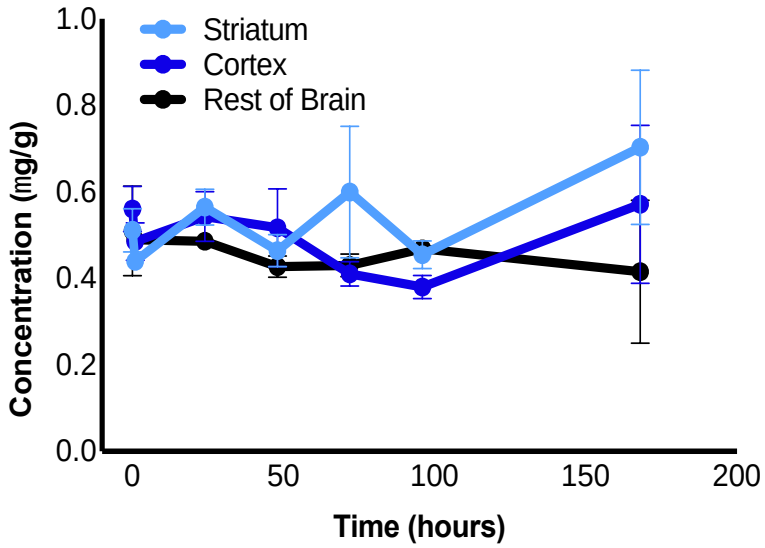

Figure S32. Time-course concentration of Gd-P1 in different brain regions. The concentration of Gd-P1 was measured in various brain regions (striatum, cortex, and rest of the brain) at different time points following tail vein injection in WT mice (n=5).

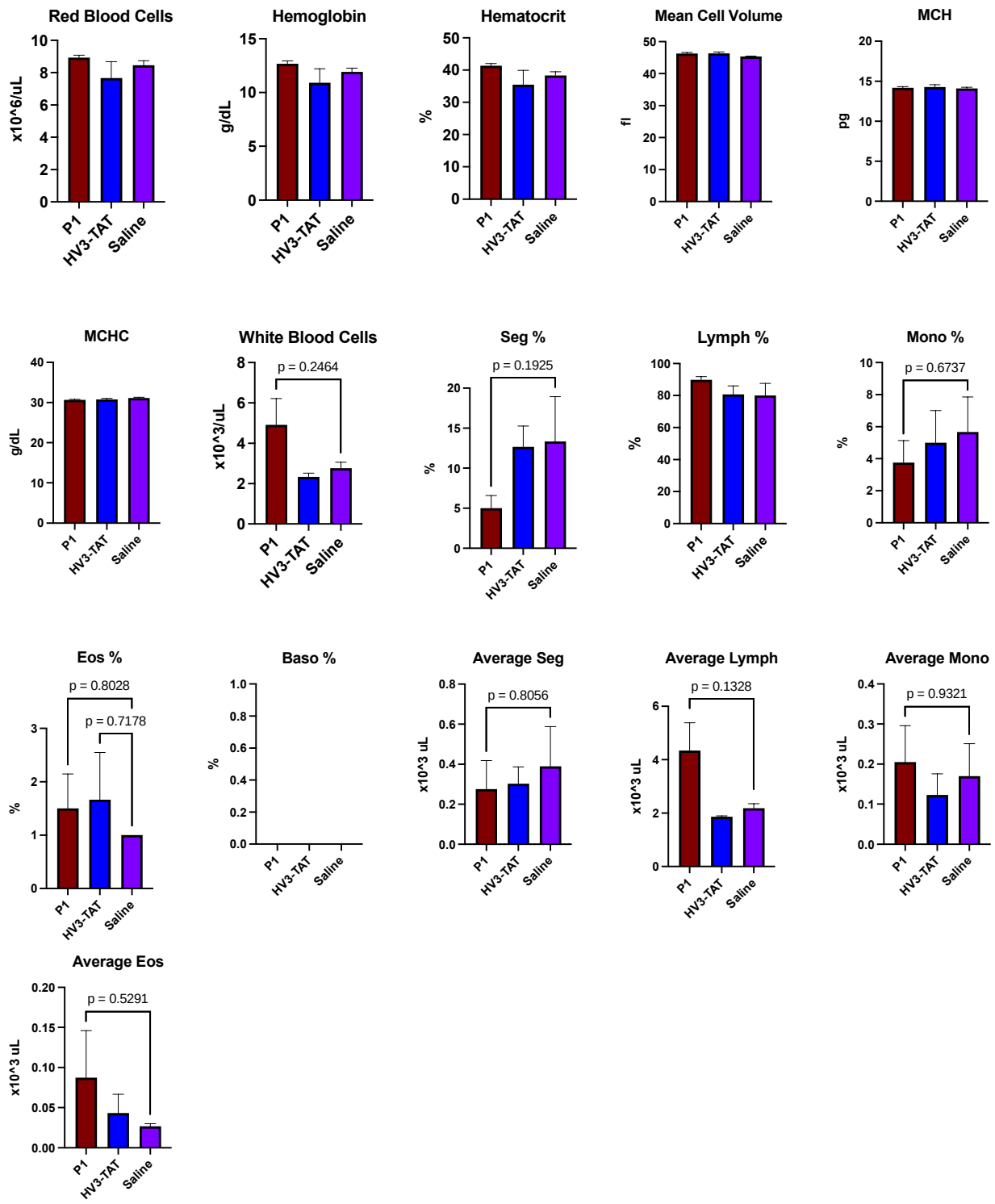

Figure S33. Complete Blood Count for Toxicity Analysis, corresponding to Supplementary Table S3. *One-way ANOVA comparisons of the mean of each group to saline (vehicle control) was used for analysis. Statistical significance was defined as follows: N.S. ($p > 0.05$), * ($p \leq 0.05$), ** ($p \leq 0.01$), *** ($p \leq 0.001$), and **** ($p \leq 0.0001$). Values are mean ± SEM.*

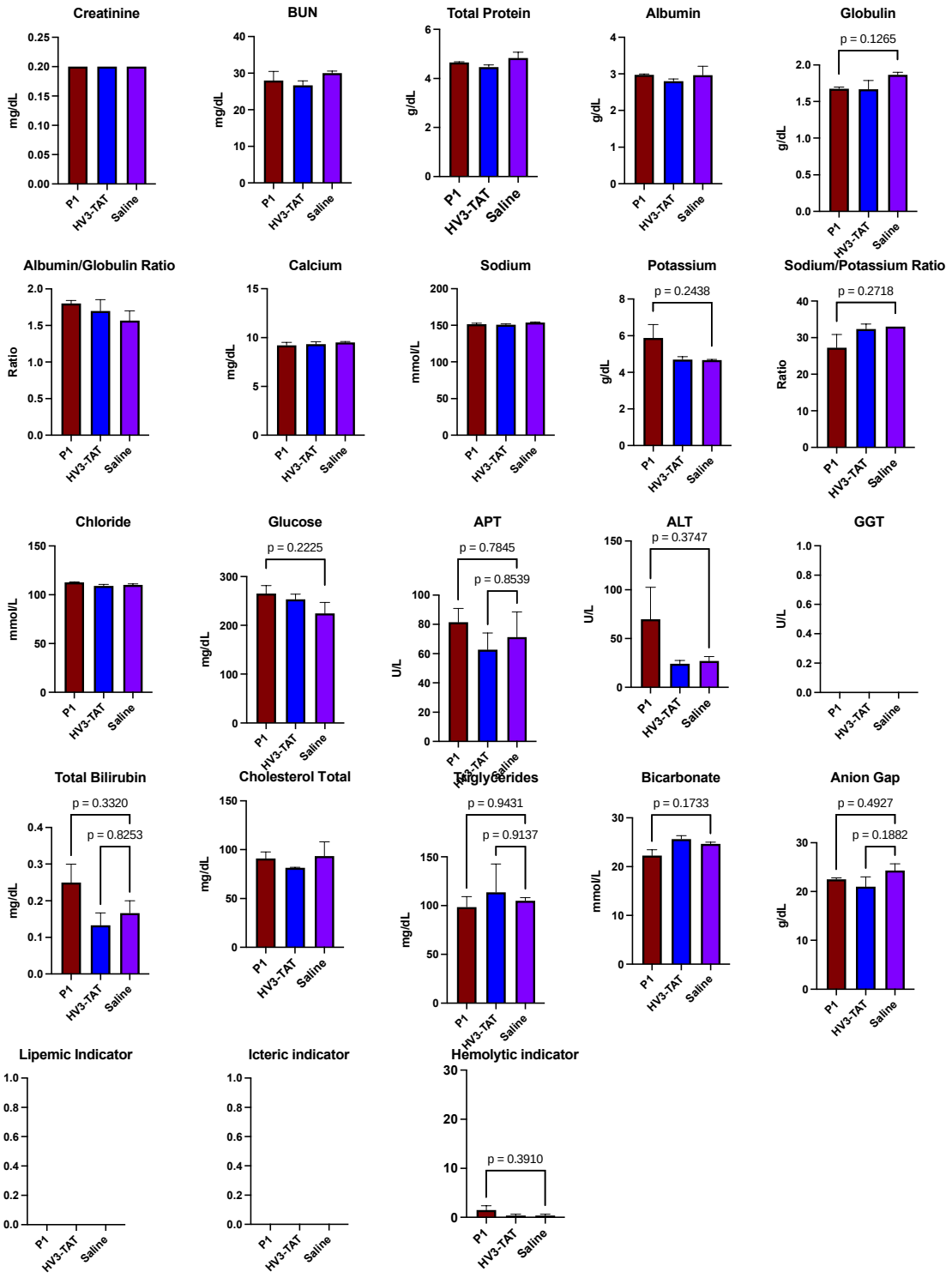

Figure S34. Blood Biochemistry Profile for Toxicity Analysis, corresponding to Supplementary Table S4. *One-way ANOVA comparisons of the mean of each group to saline (vehicle control) was used for analysis. Statistical significance was defined as follows: N.S. ($p > 0.05$), * ($p \leq 0.05$), ** ($p \leq 0.01$), *** ($p \leq 0.001$), and **** ($p \leq 0.0001$). Values are mean ± SEM.*

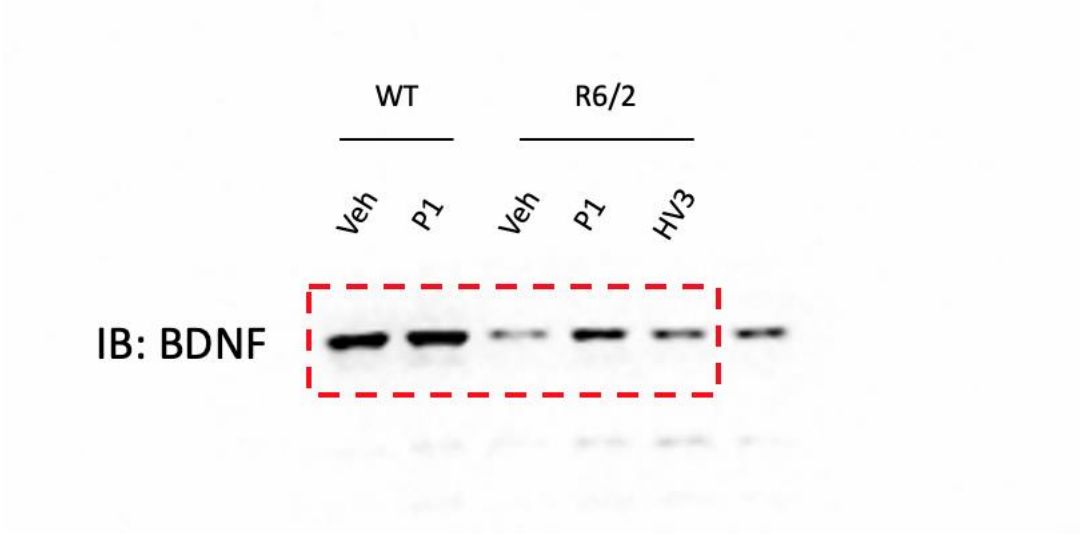

Figure S35. Full blot image of the IB: BDNF line from Fig. 6a.

Supplementary Tables

Table S1. Polymer characterization for figures

Figure	*Subfigure*	*Polymer*	*Mn*	*DP*	*Characterization*
Figure 2	a,b,f,g,	**P1**	26030	18	SEC-MALS
	c,d,e,h	**P1-Rho**	20000	14	SDS-PAGE
	I,j	**P1**	17500	12	SDS-PAGE
Figure 3	a-c				
	d-f	**P1-Gd**	14020	10	SEC-MALS
Figure 4	a-h	**P1**	16110	11	SEC-MALS
Figure 5	a-d	**P1**	20000	14	SDS-PAGE
Figure 6	a-d				

Table S2. Pharmacokinetics of P-Gd

Parameter	***Value***	***S.D.***	***C.V.***	***95% CI***		***Units***
Cle	1.06444	1.45E-01	1.36E+01	0.77354	1.35534	mL/Hr
Clp	46.36105	2.67E+00	5.77E+00	41.00497	51.71713	mL/Hr
Vc	18.8869	1.92E+00	1.02E+01	15.04366	22.73014	mL
Vp	209.9981	1.70E+01	8.10E+00	175.9207	244.0754	mL
----------	----------	**Derived Variables**	----	----------	----------	
Vss	228.885	1.73E+01	7.55E+00	194.2655	263.5044	mL
k(0,1)	0.05636	9.86E-03	1.75E+01	0.03661	0.07611	
k(1,2)	0.22077	2.39E-02	1.08E+01	0.17281	0.26873	
k(2,1)	2.45467	2.27E-01	9.24E+00	2.00011	2.90922	
	Objective	**Scaled Data Variance**				
s1 : Concentration	-1.07E+00	2.92E-01				

Total objective	-1.07E+00					
AIC	4.66E-01					
BIC	5.53E-01					

Table S3. Complete Blood Count Panel

	Saline Mouse 1	***Saline Mouse 2***	***Saline Mouse 3***	***HV3-TAT Mouse 1***	***HV3-TAT Mouse2***	***HV3-TAT Mouse 3***	***P1 Mouse 1***	***P1 Mouse 2***	***P1 Mouse 3***	***P1 Mouse 4***
Red Blood Cells (× 10^6 / μL)	8.99	8.07	8.32	5.69	8.32	9	8.92	9.31	8.92	8.61
Hemoglobin (g/dL)	12.6	11.6	11.6	8.4	11.5	12.8	12.5	13.2	13	12
Hematocrit (%)	40.6	36.8	37.6	26.8	37.9	41.7	40.7	42.7	42.2	39.8
Mean Cell Volume (fl)	45.2	45.6	45.2	47.1	45.6	46.3	45.6	45.9	47.3	46.2
MCH (pg)	14	14.4	13.9	14.8	13.8	14.2	14	14.2	14.6	13.9
MCHC (g/dL)	31	31.5	30.9	31.3	30.3	30.7	30.7	30.9	30.8	30.2
Anisocytosis	Slight	Slight	Few	Slight	Slight	Moderate	Moderate	Moderate	Slight	Slight
White Blood Cell Count (× 10^3 / μL)	2.25	2.78	3.27	2.34	2.65	2	3.82	4.43	8.68	2.71
Seg %. (%)	11	5	24	13	17	8	1	4	8	7
Lymph %.(%)	85	90	65	78	73	91	92	93	84	90
Mono %. (%)	3	4	10	7	7	1	7	2	5	1
Eos %.(%)	1	1	1	2	3	0	0	1	3	2
Baso %. (%)	0	0	0	0	0	0	0	0	0	0
A Seg. (× 10^3 / μL)	0.25	0.14	0.78	0.3	0.45	0.16	0.04	0.18	0.69	0.19
A Lymph. (× 10^3 / μL)	1.91	2.5	2.13	1.83	1.93	1.82	3.51	4.12	7.29	2.44
A Mono. (× 10^3 / μL)	0.07	0.11	0.33	0.16	0.19	0.02	0.27	0.09	0.43	0.03
A Eos. (× 10^3 / μL)	0.02	0.03	0.03	0.05	0.08	0	0	0.04	0.26	0.05
A Baso. (× 10^3 / μL)	0	0	0	0	0	0	0	0	0	0

Table S4. Blood Chemistry Panel

	Saline Mouse 1	*Saline Mouse 2*	*Saline Mouse 3*	*HV3-TAT Mouse 1*	*HV3-TAT Mouse2*	*HV3-TAT Mouse 3*	*P1 Mouse 1*	*P1 Mouse 2*	*P1 Mouse 3*	*P1 Mouse 4*
Creatinine (mg/dL)	0.2	0.2	0.2	0.2	0.2	0.2	0.2	0.2	0.2	0.2
BUN (Urea)(mg/dL)	31	30	29	29	25	26	28	32	21	31
Total Protein (g/dL)	5.2	4.9	4.4	4.3	4.6	4.5	4.7	4.7	4.6	4.6
Albumin (g/dL)	3.3	3.1	2.5	2.8	2.7	2.9	3	3	3	2.9
Globulin(g/dL)	1.9	1.8	1.9	1.5	1.9	1.6	1.7	1.7	1.6	1.7
Albumin/Globulin Ratio	1.7	1.7	1.3	1.9	1.4	1.8	1.8	1.8	1.9	1.7
Calcium (mg/dL)	9.3	9.6	9.6	9	9.8	9.2	8.5	9.1	9.6	9.7
Phosphorus (mg/dL)	6.7		8.4	6.1	7.1		7.3	8.7	8	6.9
Sodium (mmol/L)	153	155	154	151	153	149	148	150	154	154
Potassium(g/dL)	4.7	4.7	4.6	4.9	4.4	4.8	7.2	7.1	4.7	4.5
Sodium/Potassium Ratio	33	33	33	31	35	31	21	21	33	34
Chloride (mmol/L)	111	108	111	112	107	108	114	113	112	112
Glucose (mg/dL)	192	268	214	235	256	270	255	276	226	304
Alkaline Phos Total (U/L)	89	88	37	75	40	73	56	79	94	97
ALT (SGPT)(U/L)	30	33	18	24	19	30	165	62	26	26
GGT(U/L)	0	0	0	0	0	0	0	0	0	0
Total Bilirubin (mg/dL)	0.2	0.2	0.1	0.1	0.1	0.2	0.3	0.3	0.3	0.1
Cholesterol total (mg/dL)	108		79	81	82		101	100	72	91
Triglycerides (mg/dL)	109	99	107	68	106	167	86	114	75	119
Bicarbonate (TCO2)(mmol/L)	24	25	25	25	25	27	19	22	24	24
Anion Gap (g/dL)	23	27	23	19	25	19	22	22	23	23
Lipemic indicator	0	0	0	0	0	0	0	0	0	0
Icteric indicator	0	0	0	0	0	0	0	0	0	0
Hemolytic indicator	1	0	0	0	0	1	3	3	0	0

Table S5. Abbreviations for CBC and serum chemical analyses.

Abbreviation	**Description**
ALT	Alanine Aminotransferase
APT	Alkaline Phosphatase Total
Baso	Basophils
BUN	Blood Urea Nitrogen
Eos	Eosinphils
GGT	Gamma-Glutamyl Transferase
Lymph	Lymphocytes
MCH	Mean corpuscular hemoglobin
MCHC	Mean corpuscular hemoglobin concentration
Mono	Monocytes
Seg	Percentage segmented neutrophils

Table S6. Severity Scoring of Toxicity Pathology

	Treatment Group	Saline			HV3-TAT			P1			
	Animal/Slide ID	*1*	*2*	*3*	1	2	3	**1**	**2**	**3**	**4**
Tissue	**Microscopic Finding**										
Brain		0	0	0	0	0	0	0	0	0	0
Spinal cord		0	0	0	NP	0	0	0	0	0	0
Lung		0	0	0	0	0	0	0	0	0	0
Heart		0	0	0	0	0	0	0	0	0	0
Kidney	Infarct, chronic	0	0	2F	0	0	0	0	0	0	0
	Infiltrate, mononuclear cell	1M	1M	1M	0	0	0	1F	1M	1M	0
Liver	Infiltrate, mixed cell	1M	1M	2M	1M	2M	1M	1M	1M	2M	2M
Spleen	Increased pigment in histiocytes	0	0	0	0	0	0	2M	0	0	0
	Vacuolation, histiocytes	0	0	0	3M	0	0	0	0	0	0

Severity score: 0 = finding not observed; 1 = minimal; 2 = mild; 3 = moderate; 4 = marked; 5 = severe

Distribution modifier: F = focal; M = multifocal

NP = tissue not present on slide